Maisterintutkielma / Examensarbete /
Master's thesis

Materials Research
Experimental Materials Physics

Positron Annihilation at Ultralow Temperatures

Pejk Amoroso

2022

Ohjaaja (-t): / Handledare (-na): / Supervisor (-s): Jonatan Slotte
Tarkastajat: / Granskarna: / Examiners: Filip Tuomisto, Jonatan Slotte

Helsingin yliopisto / Helsingfors Universitet /University of Helsinki
Matemaattis-luonnontieteellinen tiedekunta / Matematisk-naturvetenskapliga fakulteten /
Faculty of Science

HELSINGIN YLIOPISTO
HELSINGFORS UNIVERSITET
UNIVERSITY OF HELSINKI
MATEMAATTIS-LUONNONTIETEELLINEN TIEDEKUNTA
MATEMATISK-NATURVETENSKAPLIGA FAKULTETEN
FACULTY OF SCIENCE

Tiedekunta – Fakultet – Faculty	Koulutusohjelma – Utbildningsprogram – Degree programme	
Faculty of science	Materials Research	
Opintosuunta – Studieinrikting – Study track		
Experimental Materials Physics		
Tekijä – Författare – Author		
Pejk Alex Amoroso		
Työn nimi – Arbetets titel – Title		
Positron Annihilation at Ultralow Temperatures		
Työn laji – Arbetets art – Level	Aika – Datum – Month and year	Sivumäärä – Sidoantal – Number of pages
Master's Thesis	December 2022	51

Tiivistelmä – Referat – Abstract

Positron Annihilation Spectroscopy is a powerful tool for defect characterisation, especially vacancies. Various defect properties can be studied, including defect behaviour at low and high temperatures. Despite the technique having its roots in the mid-20th century, there is little research on fundamental positron behaviour at ultralow temperatures.

In this thesis, Positron Annihilation Lifetime Spectroscopy and Doppler Broadening Spectroscopy, two sub-methods of the spectroscopy technique, were used to measure positron trap-free Ge in the temperature range of 14 mK-300 K. Since a positron trap-free sample was used, the purpose was not to study defect processes. Instead, the aim of the thesis was to investigate whether any interesting positron processes could be seen at ultralow temperatures in the annihilation data. Previous research in Al has shown no change in either lifetime or Doppler broadening below 77 K.

Measuring the positron lifetime in the sample located in a cryostat required designing a special detector setup, as the count rate was greatly reduced due to geometry. To tackle this, lifetime detectors consisting of BaF2 scintillators and quartz-windowed photomultiplier tubes were used. In addition, both analogue and digital signal processing techniques were tested for the lifetime setup, with the digital method proving to be preferable. Doppler Broadening was measured with a high-purity germanium detector connected to a digital gamma spectrometer.

The results show a decrease in S-parameter and an increase in W-parameter with decresing temprature, with the rate of change being greatest at ultralow temperatures. This behaviour is concluded to be due to incomplete positron thermalization. The positron lifetime results are more difficult to interpret, as setup challenges resulted in results of questionable accuracy. Still, the trend suggests no change in lifetime over the whole temperature interval, which is in accordance with previous research.

Avainsanat – Nyckelord – Keywords

Positron Annihilation Spectroscopy, ultralow temperature, semiconductor

Säilytyspaikka – Förvaringställe – Where deposited

Helda

Muita tietoja – Övriga uppgifter – Additional information

HELSINGIN YLIOPISTO
HELSINGFORS UNIVERSITET
UNIVERSITY OF HELSINKI
MATEMAATTIS-LUONNONTIETEELLINEN TIEDEKUNTA
MATEMATISK-NATURVETENSKAPLIGA FAKULTETEN
FACULTY OF SCIENCE

Tiedekunta – Fakultet – Faculty	Koulutusohjelma – Utbildningsprogram – Degree programme
Matematisk-Naturvetenskapliga Fakulteten	Materialforskning

Opintosuunta – Studieinrikting – Study track
Experimentell Materialfysik

Tekijä – Författare – Author
Pejk Amoroso

Työn nimi – Arbetets titel – Title
Positronannihilation i ultralåga temperaturer

Työn laji – Arbetets art – Level	Aika – Datum – Month and year	Sivumäärä – Sidoantal – Number of pages
Magisteravhandling	December 2022	51

Tiivistelmä – Referat – Abstract
Positronannihilationsspektroskopi är ett effektivt verktyg inom defektkarakteriseringsstudier, speciellt för att mäta vakanser. Olika defektegenskaper kan studeras med denna metod, såsom hur defekter beter sig i låga och i höga temperaturer. Trots att denna spektroskopiteknik har sina rötter i mitten av 1900-talet finns det begränsat med forskning i positroners beteende i ultralåga temperaturer.

I denna avhandling användes Positronannihilationlivstidsspektroskopi samt Dopplerbreddningspektroskopi, två subspektroskopitekniker, för att mäta Ge som inte innehöll positronfällor i temperaturintervallet 14 mK-300 K. Eftersom provet inte innehöll positronfällor var avsikten ej att studera defektprocesser, utan att studera ifall några intressanta positronprocesser i ultralåga temperaturer kan observeras i annihilationsdatan. I tidigare forskning gällande Al har inga förändringar i varken positronlivstid eller dopplerbreddning observerats under 77 K.

Att mäta positronlivstiden i provet inne i ett kryostat krävde en speciell detektoranordning, eftersom kryostatgeometrin resulterade i en mycket lägre pulsfrekvens än vanligt. Som åtgärd byggdes detektorer med BaF2-scintillatorer och fotomultiplikatorrör med kvartsfönster. Dessutom testades både analog och digital signalbehandlingssteknik, varav den digitala lämpade sig bättre. Dopplerbreddningen mättes med en hög-renlighetsgermaniumdetektor och en digital gammaspektrometer.

Resultaten visar en minskning i S-parameter och en ökning i W-parameter med sjunkande temperatur, där förändringen i dessa är störst i ultralåga temperaturer. Detta beteende tolkas som ett resultat av ofullständig positrontermalisation. Livstidsresultaten är svårare att tolka, eftersom svårigheterna med anordningen ledde till imprecisa mätresultat. Trenden i resultaten tyder dock på att det inte sker några förändringar i positronlivstid i hela temperatureintervallet, i enlighet med tidigare forskning.

Avainsanat – Nyckelord – Keywords
Positronannihilationsspektroskopi, ultralåg temperatur, halvledare

Säilytyspaikka – Förvaringställe – Where deposited
Helda

Muita tietoja – Övriga uppgifter – Additional information

Preface

I would like to thank Filip and Jonatan for entrusting me with this project. I was re-recruited to the lab in October 2020, to what was supposed to be a simple series of measurements that would last a few months. Instead, it turned into a two-year project with many setbacks, obstacles and stressful evenings. Still, the novel field studied in this thesis always compelled me, and I never wished I had chosen another topic. Also, this tough experimental work has taught me much more than what some simple measurements would have.

I would like to thank Jonatan, my supervisor, for helping me with the experimental work, analysis and thesis; Filip, for helping me with component planning and acquisition, theoretical questions and flexibility as my boss; Igor, Eryang and Iuliia for answering my endless stream of questions regarding the setups; Kerttuli and Pietari for helping with much of the technical aspects of the setup; and finally the whole positron group at the University of Helsinki Accelerator Laboratory for ideas and valuable discussions at our biweekly meetings.

Helsinki, November 2022
Pejk Amoroso

Contents

1 Introduction

Advances in materials are one of the major factors that have allowed the enormous progress in living standards in the past 10,000 years; the importance is even seen in the classification of human ages (stone, bronze, and iron ages). In materials science, defect characterization is critical for understanding the materials used in everyday life, such as electronics, infrastructure and power plants. Defects can change the properties of a material, even in very small quantities. Dopants are mixed into materials to alter, and hopefully improve, their properties. However, we are far from understanding all about defects and their effects. There are a large number of different types of material defects that come in different dimensions, shapes and sizes. Because of this, there are also a large number of different defect characterization techniques used in the field.

In this thesis, Positron Annihilation Spectroscopy (PAS) was used. The positron is the antiparticle of the electron; it has has equal mass and spin, and equal and opposite electric charge. The encounter of a positron and an electron results in an annihilation event, where energy and momentum is conserved [1]. In PAS, the annihilation event is recorded and analysed in various ways. It is a defect identification technique especially useful for detecting vacancies, i.e. missing atoms in a crystalline lattice.

This spectroscopy technique was used to analyse Germanium, a semiconductor, at low and ultralow temperatures, down to a temperature of 14 mK. Germanium is a material that holds importance in the field of electronics, even though many novel semiconductor materials have been discovered since the popularisation of Germanium. It is e.g. used in transistors and components for photocells.

The germanium sample measured in this thesis had low levels of impurities; consequently, these measurements do not *per se* aim to observe defect processes at low and ultralow temperatures. Instead, these experiments investigated the PAS technique at a more fundamental level. Positron annihi-

lation at ultralow temperatures remains a largely unexplored territory, which this thesis had the aim to partially cover.

Previous studies, bar one, have not found any evidence of ultralow temperatures affecting the positrons in the sample. However, measurements in these studies do not cover the temperature range 4 K-77 K. One study found, both experimentally and through calculations, evidence of an increase in positron thermalization time with decreasing temperature. In this thesis, previous work on positron annihilation at low and ultralow temperatures is expanded. Unlike most previous experiments, this work examines a semiconductor instead of a metal. Furthermore, the Doppler broadening and positron lifetime is examined closely in low temperatures (30K-100K) in addition to the ultralow temperatures.

2 Theory

The antiparticle of the electron, the positron, was predicted by Paul Dirac in 1928 in his paper "The quantum theory of the electron", for which he was awarded the Nobel prize in 1933 [2]. Combining quantum theory and special relativity, he wrote an equation that describes electrons at relativistic speeds. However, the equation has two solutions; an electron with a positive energy and one with a negative energy. Classical physics only allows positive energies, but Dirac interpreted the result as each particle having an antiparticle with opposite charge and equal mass.

In 1931, Dirac predicted the positron, a particle with equal mass as the electron, but with opposite charge [3]. He also concluded that the electron and anti-electron must annihilate upon interaction. Then, in 1932, Carl Anderson was studying showers of cosmic particles in a cloud chamber when he detected a positively charged particle with the mass of an electron. After more observations, he concluded these particles were produced alongside electrons during impact from cosmic rays. Hence, the experimental discovery of the antielectron was published in his paper "The apparent existence of easily deflectable positives" in 1932 [4]. Positron emission was discovered in 1934 by Frédérick and Irène Joliot-Curie during alpha-particle bombardment on Al, creating radioactive P that emitted particles equal to those observed by Anderson [5].

This discovery by Joliot-Curie enabled creating and using positron sources for experiments. In the 1940s, it was realized that the momentum and energy conservation in the positron-electron annihilation process can be utilized for studying electronic structure [6, 7]. In the following 20 years, two new powerful techniques emerged, Doppler Broadening Spectroscopy (DBS) and Positron Annihilation Lifetime Spectroscopy (PALS), which have been widely used for studying defects since the since the 70s.

Positrons are emitted during positive beta decay of a proton-rich radioactive nucleus along with a neutrino, and the original nucleus usually decays

into a daughter nucleus in an excited state (decay into ground state is also possible). This three-particle decay reaction results in a continuous kinetic energy spectrum for the emitted positrons. For ^{22}Na, a common positron source used in experiments, the maximum energy of the emitted positron is 540 keV [8].

The implantation profile of emitted positrons can be described empirically to be

$$P(x) = \alpha e^{-\alpha x}, \text{where } \alpha \approx 16 \frac{\rho(\text{gcm}^{-3})}{E_{max}^{1.43}(\text{MeV})}. \quad (1)$$

where ρ is the density of the material and E_{max} the maximum energy of the emitted positron [9]. By inserting E_{max} for ^{22}Na and the density of Ge, we find that the positron mean implantation depth $\frac{1}{\alpha}$ in Ge is approximately 49 µm.

2.1 Positrons in Solids

A positron entering a solid will interact with the material in various ways depending on its energy. Eventually, it annihilates with an electron. The interaction can be divided into distinct steps that affect its lifespan in the material. These are thermalization, diffusion, trapping and annihilation. The positron may also backscatter from the solid.

2.1.1 Thermalization

Positrons obtained from positive beta decay have much higher energies than the thermal energy of solids [10, 11]. Thermalization is the process when a positron loses most of its kinetic energy after entering a solid, through interactions with the electrons of the host atoms. At high positron energies, the energy loss is dominated by ionization and core-electron excitation, while conduction electron excitation and electron-hole pair production are the dominating processes at lower kinetic energies in metals and semicon-

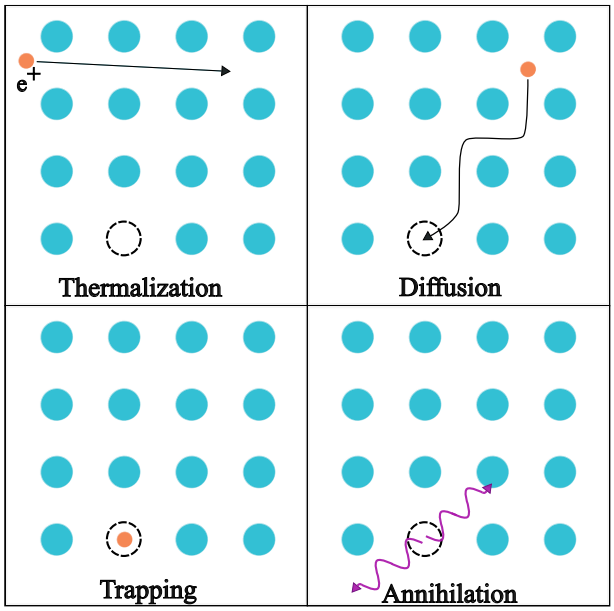

Figure 1: *Processes of a positron in a solid*

ductors respectively [12]. Finally, thermalization at near-thermal energies happens through positron-phonon scattering. After thermalization, the energy of the positron will be in the order of the thermal energy of the solid [11].

The thermalization process typically only lasts a few picoseconds in both metals and semiconductors [13, 14]. Compared to the average lifetime of a positron in a solid, which is of the order of hundreds of picoseconds, the thermalization time is a small fraction. Thus, the fraction of positrons that annihilate before completing thermalization is insignificant, and is thus usually ignored in analysis [15].

2.1.2 Diffusion

When the positron has reached the thermal energy, it will diffuse in the material as a charged particle. Due to its positive charge, it is repelled by the atomic nuclei, with positron density being highest at interstitial regions. Scattering with acoustic phonons is the most important process during diffusion, which has a temperature dependence of $\frac{1}{\sqrt{T}}$ on the diffusion coefficient [16].

The diffusion coefficient D_+ in a defect-free bulk material can be derived from diffusion theory, using the Nernst-Einstein relation and relaxation time approximation:

$$D_+ = \frac{\mu_+}{e} k_B T = \frac{k_B T}{m^*} \tau_{rel}, \tag{2}$$

where μ_+ is the mobility, k_B the Boltzmann constant, T the temperature, m_* the effective mass, and τ_{rel} the relaxation time [16]. The diffusion length in a positron-trap free lattice is

$$L_+ = \sqrt{\tau_B D_+} \tag{3}$$

where τ_B is the bulk positron lifetime. In most solids there is some concentration of defects, and the diffusion length becomes

$$L_+ = \sqrt{\tau_{eff} D_+}, \text{where } \tau_{eff} = \frac{1}{\lambda + \kappa_D}. \tag{4}$$

Here, τ_{eff} is the effective positron lifetime, λ the positron annihilation rate and κ_D the trapping rate. The presence of positron traps reduce the average diffusion length, as the diffusion time will decrease if the positron is trapped [11].

2.1.3 Trapping

Trapping is the event when a diffusing positron goes from being in a delocalised Bloch state in the crystal lattice interstitial regions to being in a localized state [17]. This is due to the positron being positively charged, thus being repulsed by atomic nuclei. A typical positron trap is thus an open-volume defect, such as a vacancy where the repulsion is lower. The positron sees this as a potential well and thus transitions into a localized state.

For trapping to be observable in an experiment, the concentration of positron traps has to been sufficiently high so that the change in positron lifetime is observable. This is due to trapping-annihilation events compete with annihilation events without trapping. Positron traps increase the positron lifetime, and decreases diffusion length.

The defect trapping rate is given by

$$\kappa_D = \mu_D c_D \tag{5}$$

where μ_D is the defect specific trapping coefficient and c_D is the defect concentration in the material [15].

2.1.4 Annihilation

When a positron eventually annihilates with an electron, the most common outcome is the emission of two photons in opposite directions. Energy and momentum conservation dictates that the photon pair has a minimum combined energy of 1.022 MeV, which is the resting energy of an electron-positron pair (2×511 keV).

The positron annihilation rate λ, which is the inverse of the positron lifetime τ, is given by

$$\lambda = \frac{1}{\tau} = \pi r_0^2 c \int |\psi_+(\mathbf{r})|^2 n_-(\mathbf{r}) dr, \tag{6}$$

where r_0 is the classical electron radius, c is the speed of light, $\psi_+(r)$ is the

positron wave function, and $n_-(r)$ is the electron density [17].

After the positron has thermalized in the solid, it has a negligible momentum compared to that of the electrons. Hence, the momentum of the annihilation photons gives the electron momentum distribution at the annihilation site. An approximation of the annihilation radiation momentum distribution can be expressed as follows:

$$\rho(\mathbf{p}) = \pi r_e^2 c \sum_i |\int d\mathbf{r} e^{-i\mathbf{p}\cdot\mathbf{r}} \psi_+(\mathbf{r})\psi_i(\mathbf{r})|^2, \tag{7}$$

where i denotes the occupied electron states [17].

2.1.5 Backscattering

Positrons hitting the surface of a solid can backscatter from the surface through elastic scattering from the solid's nuclei. The event probability is determined by the scattering material and the incident positron's energy. P U Arifov et al. [18] measured the total positron backscattering coefficient η_+ for atomic mass numbers $4 \leq Z \leq 82$, and found a dependence on the atomic mass number Z described by

$$\eta_+ = 0.0194 Z^{0.7004}. \tag{8}$$

This proportional increase in positron backscattering coefficient with increasing atomic mass number has to be considered in analysis, to which we will return later in this thesis.

2.1.6 Positronium

Although positrons usually annihilate with electrons, thermalized positrons may also form a short-lived hydrogen-like atom. Due to their opposite charge, there is a possibility that the positron and electron form a bound state by electromagnetic interaction. However, even if from an electromagnetic

point of view the bound state is stable, quantum mechanically the two wave-functions will overlap, resulting in an annihilation event.

Two spin states of positronium are known; para-positronium and ortho-positronium. The former is in a singlet state; the positron and electron have antiparalell spin, resulting in a system spin of $S = 0$. The mean-lifetime is in the order of 10^{-10} s, after which the positron eventually annihilates with the electron. The annihilation of para-positronium results in the emission of an even number of photons. Ortho-positronium is a triplet state; the positron and electron have parallel spin, resulting in $S = 1$. This positronium state has a mean-life in the order of 10^{-7} s and the annihilation event results in the emission of an odd number of photons. Para-positronium usually decays into two photons, and ortho-positronium into three. The probabilities of para-positronium decaying into four photons and ortho-positronium decaying into five photons are of the order of 10^{-6}. Hence, these rare events are usually ignored [19].

2.2 Defects in Semiconductors

Semiconductors are the era-defining materials in the information age that is the 21st century. Used in essentially all electronics, understanding their behaviour under different conditions allows for improved performance. What makes these materials so useful is the ability to tune their properties by introducing defects. By introducing lattice defects into the crystal structure, known as doping, one can control the electronic, optic and other elemental properties of the material.

Defects in semiconductors are found in quantities much smaller than the host atoms. In crystalline solids, defects are defined as disruptions in the periodicity of the crystal structure. Defects can be classified by their dimensionality. Zero-dimensional defects are called point defects, and do not extend past a point location in the crystal. Examples of point defects are vacancies and interstitials. Following the same logic, there are one-dimensional or

line defects, such as edge and screw dislocations; two dimensional or surface defects, such as grain boundaries; and three-dimensional or volume defects, such as aggregates of impurities. The presence of one of these types of defects does not exclude other types of defects in the lattice. Furthermore, a certain defect can result in the formation of another type of defect [1, 17].

Compared to e.g. metals, defects have a much larger impact on the material's properties. Even though dopants are introduced under controlled conditions to achieve desired properties, it is challenging to stop other defects from forming. Because even a small amount of defects can have a significant impact on properties, it is important to identify and understand the defects and their behaviour [1].

2.2.1 Positrons in Semiconductors

In a perfect periodic crystal lattice of a semiconductor, a thermalized positron is in a Bloch-like state. The ground-state positron can be described by the single-particle Schrödinger equation

$$-\frac{1}{2m^*}\nabla^2\Psi_+(r) + V(r)\Psi_+(r) = E_+\Psi_+(r) \tag{9}$$

where the positron potential $V(r)$ is a factor of the electrostatic Coulomb potential from positively-charged nuclei and a term based on electron-positron correlation effects. Because of the former interaction, the wave function is concentrated in the interstitial space where the Coulomb repulsion is at a minimum.

Positron trapping in semiconductors, especially compound semiconductors, is less trivial than in metals. This is because positrons are sensitive to charged point defects, of which (compound) semiconductors have a much larger variety. Positively charged defects are invisible to positron techniques due to repulsion, while the sensitivity for neutral defects is similar to that in metals. Positrons are most sensitive to negatively charged open-volume defects [11]. It is possible distinguish neutral from negatively charged vacan-

cies by examining the temperature dependence, since positron trapping into neutral vacancies is temperature independent while trapping into negative vacancies is not [1].

In addition to open-volume defects, negatively charged non-open-volume defects also act as positron traps. Examples of these are acceptor impurities in p-type semiconductors or negatively charged antisites in compound semiconductors. Positrons may bind weakly to these centers, which thus are called shallow positron traps. In conclusion, neutral and negatively charged open-volume point defects, and negative ions are the strongest zero-dimensional positron traps in semiconductor materials [11].

2.3 Positron Annihilation Spectroscopy

PAS techniques can be divided into two categories, "slow" positron techniques and "fast" positron techniques. Fast positron techniques use unmoderated positrons, with the broad kinetic energy spectrum discussed previously. Because the mean implantation depth of a "fast" positron from an encapsulated source is approximately 50 µm, fast positron experiment techniques can only investigate bulk properties of materials.

There are two main fast-positron techniques; PALS which measures the lifetime of the positron in the sample material, and DBS which measures the electron momentum distribution.

Slow positron beams use positrons that have been slowed down, and then accelerate them. Typically, the positrons are slowed down with a moderator, a thin layer of a material which has a negative work function for the positron. The moderator is placed in front of the positron source. Mono-energetic positrons then emerge from the other side of the moderator, and can be accelerated to a desired energy. Consequently, the implantation depth can be controlled accurately. Slow positron beams are therefore useful for studying thin layers and surfaces. Moderating the positrons results in a much lower count rate than in unmoderated positron setups. Thus, positron sources for

slow positron beams have a much higher activity than sources used in fast positron setups.

In laboratory settings, positrons are usually obtained from the β^+ decay of radioactive isotopes. The most commonly used positron source is ^{22}Na, for which the decay can be described by

$$^{22}\mathrm{Na} \rightarrow ^{22}\mathrm{Ne} + e^+ + \nu_e + \gamma \tag{10}$$

^{22}Na has a relatively low emission intensity of up to 10^9 positrons/s. However, its half-life of 2.6 y and a positron yield of 90.6 %, makes it a suitable positron source in PAS, since the same source can be used for many years [20].

2.3.1 Doppler Broadening Spectroscopy

Doppler Broadening Spectroscopy is a technique used for measuring the electron momentum distribution. Because it is not a time-dependent technique, it is used in both slow-positron beams and sample-source-sample measurements.

The momentum of the positron is negligible to that of the electron. Thus, the electron momentum component in the propagation direction of the annihilation photon results in a Doppler shift in the annihilation photon's energy of 511 keV. The relation between the longitudinal momentum component $\mathrm{p_z}$ and the energy shift can be written as

$$\Delta E = \frac{p_z c}{2}, \tag{11}$$

where

$$\rho(p_z) = \iint dp_x dp_y \rho(\mathbf{p}.) \tag{12}$$

Analysis of the momentum distribution peak is done by defining two parameters that describe the shape of the peak. The S-parameter (shape) describes the low-momentum electrons, which are seen at the center of the

annihilation line. It is calculated as the ratio of counts in the chosen range to the total count amount. Similarly, the W-parameter (wing) is defined as the edges of the annihilation line, namely the high-momentum electrons.

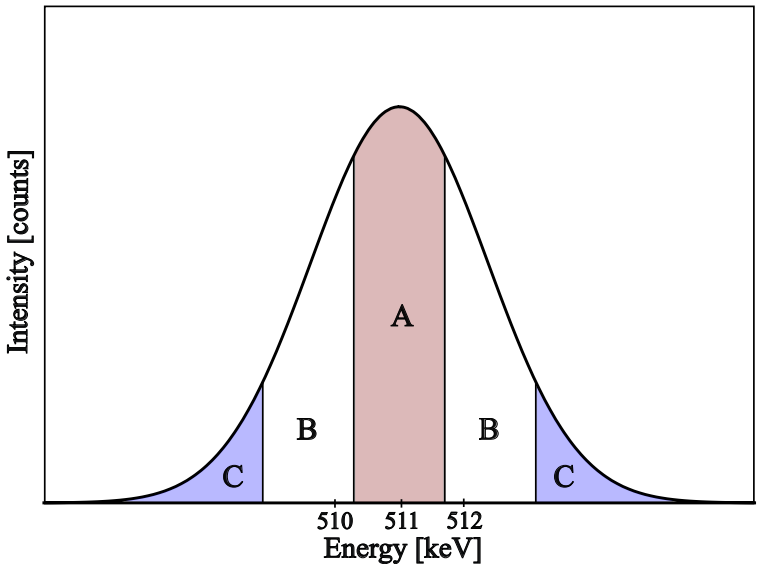

Figure 2: *Background-reduced annihilation peak diagram showing the calculation method for the S- and W-parameter. The* 510 keV *and* 512 keV *locations on the energy axis are approximate, and vary depending on the width of the peak.*

To calculate the S- and W-parameter, we define certain areas of the peak according to Figure 2. The S-parameter is calculated as follows:

$$S = \frac{A}{A + B + C} \tag{13}$$

and the W-parameter similarly

$$W = \frac{C}{A + B + C}. \tag{14}$$

Since the ranges over which the parameters are calculated are chosen by the researcher, the absolute value does not say anything in itself; it is the

change in the parameter value that is investigated. Furthermore, the absolute values of the S- and W-parameters also depend on many other variables, such as detector resolution, geometry and Multichannel Analyser (MCA) channel width.

As with any measurement technique, the statistical error has to be considered. The statistical error of the S-parameter is given by

$$\delta S = \sqrt{S\frac{1-S}{N}} \tag{15}$$

where N is the total amount of counts in the peak. The statistical error $\delta W$of the W-parameter is calculated in the same manner, by substituting S with W. Naturally, more counts result in smaller statistical error.

2.3.2 Positron Annihilation Lifetime Spectroscopy

When ^{22}Na decays, a positron and a neutrino are emitted. In addition, the daughter nucleus, ^{22}Ne, is left in an excited state with a half-life of 3.7 ps. When the nucleus transitions to its ground state, a 1.275 MeV gamma photon is emitted. Due to the short half-life of the excited state compared to the lifetime of a positron in a solid, the decay gamma photon is treated as being emitted simultaneously to the positron. Hence, the decay time is ignored in analysis.

PALS setups consist of two or more detectors, which measure both the emitted 1.275 MeV gamma photon and the 511 keV gamma photon emitted due to annihilation between the positron and an electron in the sample. Using various methods, the time difference between the start event and stop event can be extracted.

Positrons are most sensitive to open-volume defects, such as vacancies. Measuring the positron lifetime in a sample with defects will yield a deviation from a defect-free value; thus, measuring the lifetime is a good technique to estimate the type and amount of open-volume defects present in the sample.

Trapping of positrons in the sample is described with kinetic equations, from which one can derive the positron lifetime probability distribution:

$$n(t) = \sum_i I_i exp(-\lambda_i t), \tag{16}$$

where I_i are the intensities and λ_i the annihilation rates of the different annihilation events, also known as lifetime components.

In PALS, the most important experimental quantity that is measured is the average positron lifetime. The average lifetime is independent of trapping model, and can thus be found from the spectrum without knowledge of the decomposition.

2.4 Previous Work

During the research for this thesis, only four articles were found that could provide insight and serve as comparison for the experiments conducted here.

G. M. Hood et al. studied ultra-pure, well-annealed Al at 77 K-293 K, P. J. Schultz et al. at 85 mK-300 K, and T. Troev et al. at 12 mK-300 K, using DBS [21–23]. A common finding in these three experiments was that the S-parameter increases linearly above 77 K. It was concluded that this was due to thermal expansion, as the S-parameter increase scales to that of the static thermal expansion coefficient. It should be noted that the point where the S-parameter increase begins, 77 K, is not necessarily the actual temperature where the S-parameter increase starts, but the limit of the cooling system used. The cooling systems in question use liquid nitrogen (LN_2), which has a boiling point of 77 K.

P. J. Scultz et al. and T. Troev et al. saw no change in the S-parameter below 77 K. However, there are no measurements done between 4 K and 77 K, again due to cooling system limitations. Thus, any possible processes that might cause changes in the behaviour of the S-parameter in this temperature gap could not be observed. Still, from their results below 4 K and above 77 K

it was concluded that there were no signs of positron localisation [22, 23].

P. J. Scultz et al. and T. Troev et al. also measured the positron lifetime with the same setup and parameters. No obvious changes in positron lifetime were observed. However, it was indicated that the results should be analysed with caution. The geometry of the setup statistically limited the results, as the cryostat where the sample was located significantly increased the distance between lifetime detectors, and thus resulted in a low amount of counts. The Doppler broadening setup was much less limited by distance, and the results reported are statistically much more reliable.

Nissilä et al. [24] calculated the positron thermalization time in Si and GaAs down to 4 K by numerically solving the Boltzmann equation for the positron momentum distribution. They found variations in thermalization time due to differences in the strength of positron-phonon coupling. They also found experimental evidence of incomplete thermalization already in a temperature range of 50 K-100 K. Their calculations also seem to suggest a thermalization time in the order of nanoseconds at temperatures below 1 K.

3 Experimental Method

Due to the little previous research on this topic, and thus a factor of unpredictability as to what we could expect to see during this experiment, we opted to simultaneously conduct PALS and Doppler Broadening Spectroscopy measurements. The PALS measurement setup consists of two detectors, a digital oscilloscope and a PC. The detectors consisted of a scintillator crystal and a photomultiplier tube, which were operated at high voltage. The Doppler Broadening was measured using a High-Purity Germanium (HPGe) detector operated at 77 K (cooled down using liquid nitrogen, LN_2), which was connected to a digital gamma spectrometer (Ortec DSPEC jr. 2.0).

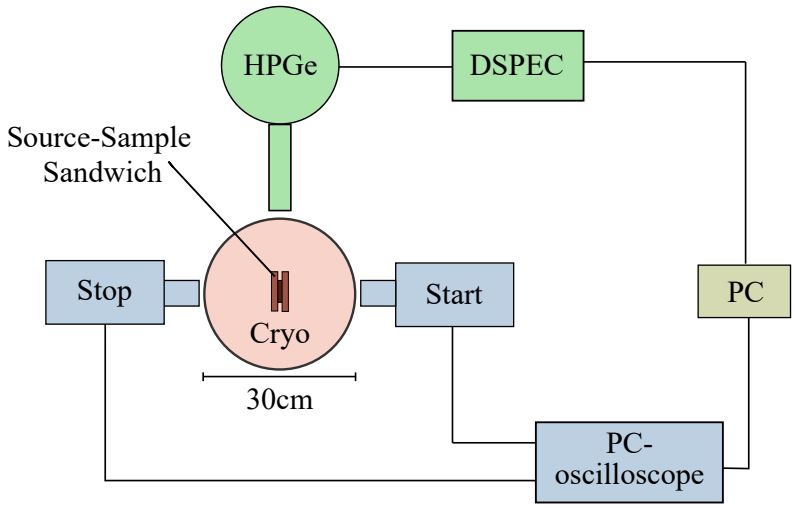

Figure 3: *Experimental setup with digital signal processing. PALS components are coloured in blue, and Doppler Broadening components in green.*

The positron lifetime detectors were positioned in line with the sample-source-sample direction, while the HPGe-detector was positioned perpendicular to this line. For measurements below 4 K, the distance between the positron lifetime detectors was 30.4 cm, due to the 30.0 cm diameter of the

cryogen-free dilution refrigerator. For measurements above 4 K, we could reduce the detector-detector distance to 1.0 cm.

Minimising distance from the source to detectors is important in order to maximise count rate. The count rate decreases by a factor of $\frac{1}{d^2}$ where d is the distance, meaning that doubling the distance decreases the count rate four-fold.

3.1 Sample-Source Sandwich

The sample measured in this thesis was positron trap-free Germanium. The Ge was cut into two similarly-sized rectangles with a size of approximately 8 mm × 8 mm. When cutting the sample, the size should be chosen such that the source does not protrude over the sample edges, and such that the sample-source package fits into the cooling system.

The positron source was made by placing a small amount of ^{22}NaCl diluted in HCl-water solution on top of a piece of Al foil of thickness 0.0015 mm. A heating lamp was used evaporate the HCl solution, leaving a layer of ^{22}Na salt on the foil. The foil was then folded in such a manner that the salt was securely enclosed. The positron source was placed between the two sample pieces, in this case Ge. If the sample has surfaces of different roughness, the smoother side should be placed towards the source as it reduces surface area and thus backscattering. The sample-source package was then enclosed in Al foil of thickness 0.63 mm (normal kitchen Al foil). This was done as an extra precaution, as it further prevents salt leakage into the setup. This was especially important in this case, as radioactive contamination in the cryostat could damage it. Finally, the sample-source package was placed in a copper sample holder. The sample-source geometry is usually called a sandwich, a name which derives from the geometry, as seen in Fig. 4.

Two positron sources were used for the experiments. The first one had an activity of 3.6 MBq, and was used for the measurements done at 14 mK-3.7 K. The same source would normally have been used for the remainder of

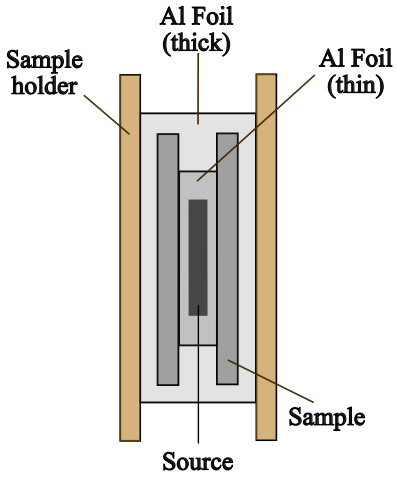

Figure 4: *Schematic diagram showing the composition of the sandwich.*

the measurements. However, the source was damaged during opening of the sandwich. The second positron source had an activity of 2.2 MBq. A typical positron source used for lifetime spectroscopy is between 0.3 MBq - 1 MBq.

Source-making for positron lifetime measurements requires evaluating the purpose and needs of the experiment, and then compromising between count rate and resolution. Using a very active source increases the count rate, but also increases the probability of two or more positrons co-existing in the sample. One of the fundamental assumptions of the standard trapping model in PALS is that only one positron is present in the solid at any time. If there is more than one positron in the sample at a given time, their annihilation events will occur close to each other in time, and the signal processing system cannot distinguish between the annihilation events. Thus, background increases if the source is too active. In addition, a larger salt volume also increases the fraction of annihilation events occurring in the source itself. However, this negative effect is much less significant than the aforementioned.

However, an unusually active source was used in these experiments due to the geometry and problems with signal processing; the high activity of

the source was not a problem as the number of positrons entering the sample is greatly reduced by distance, and signal processing problems significantly reduced the count rate further.

3.2 Lifetime Spectroscopy

3.2.1 Scintillator Crystal

Scintillators are commonly used in particle physics for radiation detection purposes. A scintillator is a material that exhibits the phenomenon of scintillation; when hit by ionizing radiation, such as X-rays or gamma rays, the particle's energy is converted into visible or near-visible light [25].

Scintillators come in many forms; gaseous, liquid or solid, and organic and inorganic. They are usually coupled to photodetectors, such as photomultiplier tubes or photodiodes, to form radiation detectors. Like in any device, the scintillator material is chosen to suit the application. Scintillators vary greatly in phase, size, cost, and importantly advantageous and disadvantageous properties. In PALS, time resolution is one of the more important properties to consider [25].

In PALS, inorganic plastic scintillators are most commonly used due to their cheap price and reasonable quantum efficiency [25]. Initially, plastic scintillators were used, since they are the standard choice at the University of Helsinki Accelerator Laboratory, but testing showed the unusual experimental geometry required a different type of scintillator crystal. The unusually long distance between detectors, due to the cryostat, resulted in a low count rate. Especially the higher energy, positive beta decay gamma peak (1.275 MeV) was indistinguishable from the background, as plastic scintillators have a low quantum efficiency at these energies. Thus, the scintillators were changed to Barium Fluoride (BaF_2) scintillators, which have a higher quantum efficiency at high energies.

BaF_2 is one of the fastest scintillator materials. It has two emission com-

ponents; a fast component with an emission maximum at 220 nm and a decay time of 0.8 ns, and a slow component with an emission maximum at 315 nm and a decay time of 630 ns [26]. Approximately 15 % of photoelectrons are produced by the fast component, and 85 % by the slow component. BaF_2 has low self-absorption, enabling the usage of large crystals to increase the count rate [27]. Typically only the fast component is used, as BaF_2 scintillators are selected in applications where high time resolution is needed [25]. However, in this setup both the fast and slow components were used to maximise the count rate.

BaF_2 is a material with high density compared to plastic scintillators ($4.9\,g/cm^3$ vs $1.0\,g/cm^3$[28, 29]). This brings the upside of high photon yield, but also results in a non-negligible fraction of backscattered photons. As a result, the sandwich should be placed as seen in Fig. 5; the sandwich is between the detectors, but out of the common scintillator axis by a minimum distance of the scintillator radius. This also reduces simultaneous detection of both annihilation photons [30].

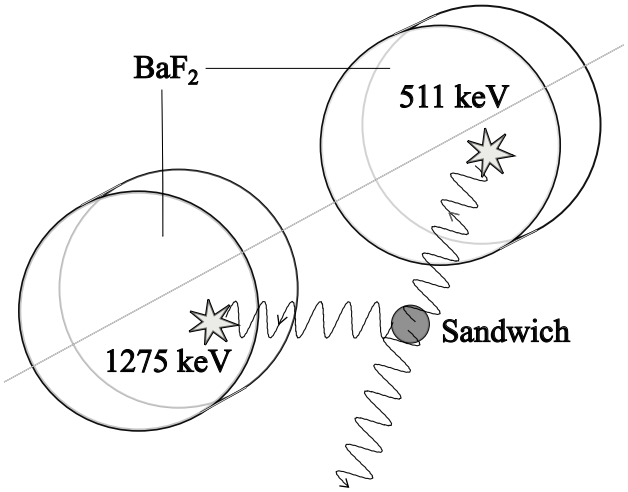

Figure 5: *Diagram showing the placement of the sandwich and detectors. Line represents the common axis of the centres of the scintillators.*

The scintillators were wrapped in PTFE (teflon) tape and protective aluminised mylar foil. The PTFE tape acts as a reflector; it improves the total output of the scintillator, thus increasing the count rate [31]. The scintillators are coupled to the photomultiplier tubes using silicone grease. An important aspect when selecting the type of grease is to choose one with similar refractive index in order to minimise signal loss, especially when using BaF_2 scintillators, as the fast scintillation component is blocked by many of the commonly used types of grease [32]. Finally, the scintillators were covered with duralumin cups and taped to the photomultiplier tubes with electrical tape. The duralumin cups provide water-proof housing, which is important since BaF_2-scintillators are slightly hygroscopic (moisture-absorbing).

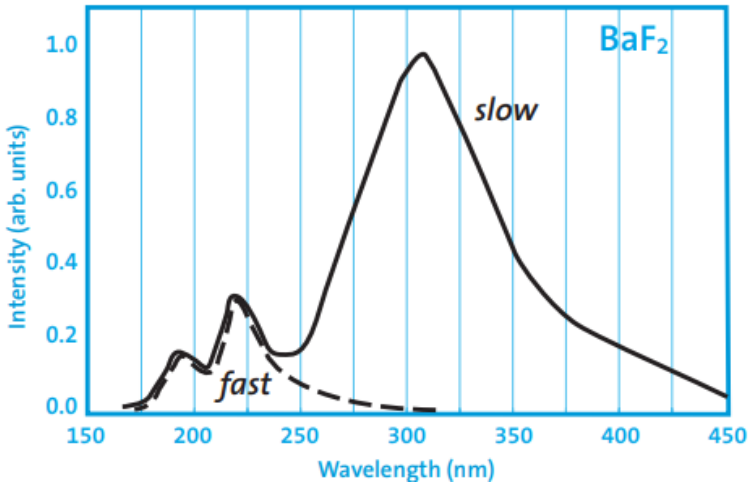

Figure 6: *BaF_2 scintillation emission spectrum. Both the fast and slow emission components are marked.* [27]

3.2.2 Photomultiplier Tube

Photomultiplier tubes (PMTs) are commonly used for detecting weak (low energy, long wavelength) light signals, in areas such as astronomy or particle physics. The PMT converts the photon to an electrical signal. A PMT

consists of a photosensitive cathode, which emits electrons when struck by photons. Following the cathode, a series of dynodes multiply the number of electrons, greatly increasing the magnitude of the signal, up to a million-fold amplification. There are various types of PMTs, including with varying quantum efficiency, wavelength absorption range an so forth [25].

Hamamatsu R3378-51 PMTs were used in this experiment. The choice was based on the fact that BaF_2 scintillators emit light in the near-visible range, which is absorbed by regular glass. Thus, BaF_2 scintillators should be paired with PMTs with quartz-windows, that do not absorb near-visible light. The PMTs have spectral response in the wavelength range 160 nm-650 nm [33].

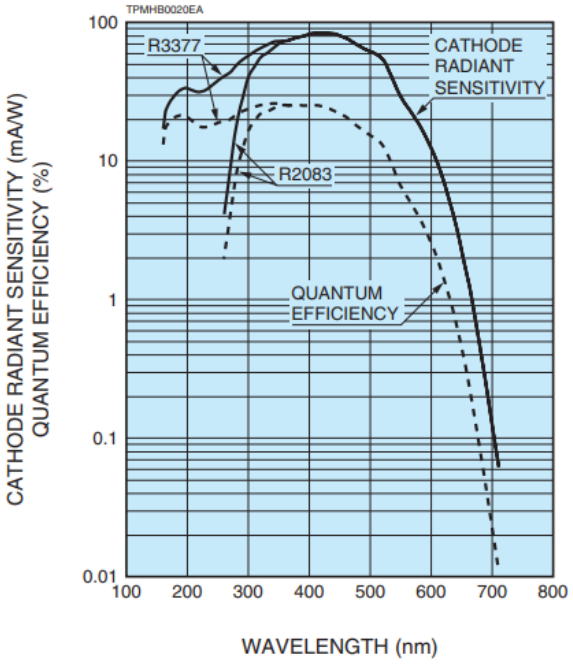

Figure 7: *Hamamatsu R3378 PMT quantum efficiency. Model R3377 is the non-built-in version of the R3378. The R3378 has high quantum efficiency at wavelengths of photons emitted by BaF_2.* [33]

The standard supply voltage by the manufacturer for this PMT model is

3000V, with a maximum of 3500V [34]. The supply voltages for the detectors used in the experiments were 2650V and 3350V. The supply voltage was selected such that the output signal from the PMTs had an amplitude of 1.5 V-2.0 V. Since the PMTs had very different anode luminous sensivity, the voltages also differed from each other.

3.2.3 Signal Processing

Determining the best way to process the lifetime signal took considerable time, as there are advantages and disadvantages with both analogue and digitals setups. Initially, a digital oscilloscope (Picoscope series 6000) was used to collect and process the raw data from the detectors, as this was standard procedure in the University of Helsinki Accelerator Laboratory. However, after a series of test measurements, it was noticed that the signal filtering made by the digital oscilloscope was flawed, as the count rate was two to three times lower than expected. Thus, a decision was made to switch to analogue signal processing equipment. After optimization and calibration, the count rate was roughly doubled; from about 50 cps using digital equipment to 110 cps with analogue.

The detector signals were led into constant-fraction discriminators (CFDs), which suppress noise and generate standard timing pulses. The start pulse was fed straight into a time-to-amplitude (TAC) converter, and the stop signal through a delay box into the TAC. The TAC produces a signal with an amplitude proportional to the time difference between start- and stop-signals. A multichannel analyser compiles the TAC-signals into a lifetime spectrum.

However, further problems emerged during testing. Even though the total count rate had improved, the desired signal shape was not achieved. It was discovered that this was since the PMT anode luminous sensitivities were very different, 610 A/lm and 226 A/lm [34], which in turn meant the signals emerging from the PMTs were different. Processing the signals using the analogue equipment to make them readable by the software was too difficult

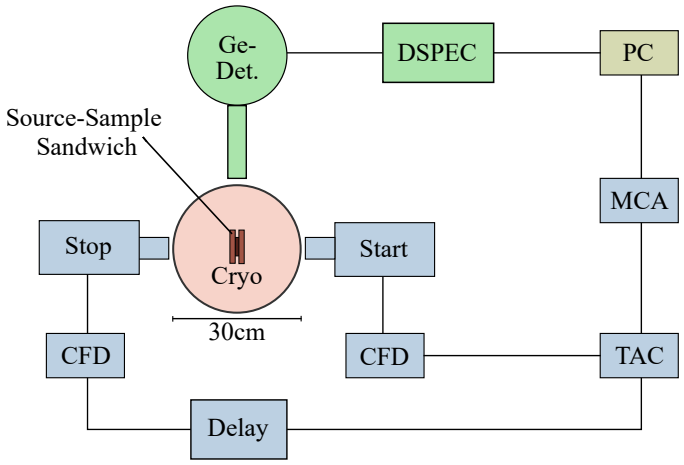

Figure 8: *Experimental Setup with analogue signal processing. PALS components are coloured in blue, and Doppler Broadening components in green.*

and time-consuming, so the signal processing method had to be switched back to the digital oscilloscope.

The software used for signal processing, called eLab, is a 'home-made' program. The program was written to be used with the standard lifetime detectors in the University of Helsinki Accelerator laboratory, which use plastic scintillators. The emission spectra and signal shape is different from that of the BaF_2 scintillators that were used in the experiments of this thesis, and thus the software is not optimized for the BaF_2 signal. It is worth noting that the software is not completely optimized for the plastic scintillator detectors either, as the count rate is lower than in analogue setups.

The software settings that normally are used for the Accelerator Laboratory setups were not compatible with the new detectors. Changing detector voltage or any of the standard software settings resulted in one of three results; a signal from the start detector, a signal from the stop detector, or

no signal from either detector. This was a puzzling problem, as clear signals could be seen on an oscilloscope.

The final solution was one in which the logic still is unclear to the author; by choosing both the start signal and the stop signal as triggers, and using both as pulse width qualifiers, a signal from both detectors could finally be recorded. Potential explanations to this are either that the signal shapes were too different due to different pulse heights or the two different, fast and slow, signals. The problem could most likely be explained and solved by thoroughly analysing the software code.

Energy window selection is an important part of PALS. The emitted energy is a continuous spectrum consisting of three main components; the Compton background, the annihilation peak and the decay photon peak. The peak resolution depends largely on the scintillator material.

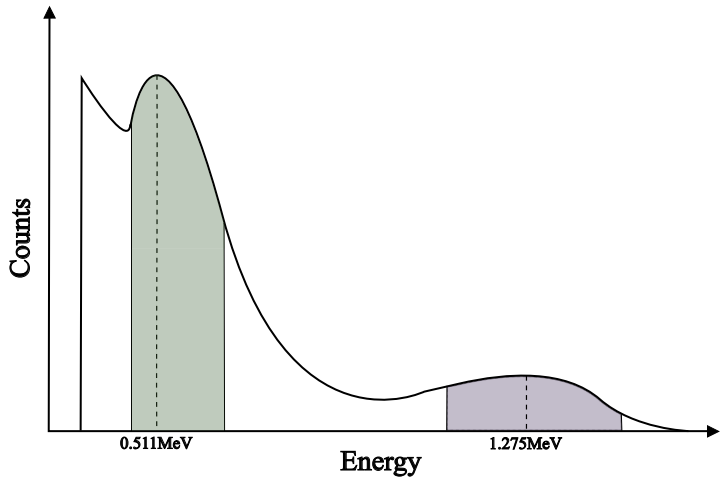

Figure 9: *Energy window selection. Peak placement, shape and size all vary depending on setup. Energy windows may be broader or narrower.*

When selecting which area of the spectrum to use for lifetime analysis, one has to find a suitable balance between count rate and resolution. The narrower the selected energy windows are, the better the energy resolution is (in general). However, choosing a narrow area reduces the count rate. In

this work, because of the geometry-limited count rate, wider energy windows were chosen.

The resolution of the positron lifetime setup was measured using ^{60}Co as a photon peak source, a commonly used method. From the measured energy peak, a gaussian curve is fitted, in this case using Origin Pro, after which the Full Width Half-Maxumum (FWHM) is calculated. The resolution of the PALS setup was 280 ps.

3.3 Doppler Broadening Spectroscopy

3.3.1 High-purity Germanium Detector

The annihilation gamma photons were detected using a BSI High-Purity Germanium (HPGe) detector. HPGe detectors possess high energy resolution and are easy to set up and use, making them a commonly used radiation detector [25]. The detector is cryogenically cooled using liquid nitrogen (LN2) to 77 K to maximise efficiency, as operating at room temperature would result in high levels of noise due to thermal excitations. As gamma photons pass through the germanium crystal, electron-hole pairs are created in the process. The number of electron-hole pairs is proportional to the energy of the gamma photon. Using an electric field, the electrons and holes are directed to electrodes, resulting in a pulse with an amplitude proportional to the gamma photon energy, which then is recorded.

3.3.2 Signal Processing

The pulses from the HPGe-detector were recorded using the multichannel analyzer software Ortec Maestro 7.0. Before starting measurements on the sample, the detector and software were calibrated. This was done by tuning the fine and coarse gain until the 511 keV annihilation peak is centered at channel 4000. Channel 4000 is chosen for convenience; the maximum channel is 8042, placing 4000 roughly in the middle of the recorded spectrum. Once

the gain has been tuned, the gain stabilizer is turned on to center the peak and decrease the resolution.

Next, the resolution is measured and calculated. The resolution of HPGe-detectors is often defined as the FWHM of the ^{137}Cs photon emission peak. Thus, a ^{137}Cs radioactive source is placed next to the positron source. The positron annihilation peak of 511 keV and the ^{137}Cs emitted photon with an energy of 662 keV are both used for resolution calculation. The calculation is done followingly:

$$\mathrm{FWHM}_{E_2}[keV] = \sqrt{\frac{E_1}{E_2}} \times \frac{E_2 - E_1}{\mathrm{P}_{E_2} - \mathrm{P}_{E_1}[ch]} \times \mathrm{FWHM}_{E_2}[ch], \qquad (17)$$

where E_1 is the annihilation photon energy (511 keV), E_2 is the ^{137}Cs photon energy (662 keV), P_{E_1} and P_{E_2} are the peak center channel numbers of respective photon peak, and FWHM_{E_2} is the software-given FWHM of the ^{137}Cs peak in channels. This equation yielded a resolution of xxx.

3.4 Temperature control

3.4.1 Cryogen-free dilution refrigerator

The first stage of measurements were in the temperature interval 14 mK-3.7 K. The system used to cool the samples to these ultracool temperatures was a Bluefors model SD250 cryogen-free dilution refrigerator system. Cryogen-free (or dry) dilution refrigerators are a more modern version of the classic (or wet) dilution refrigerators. Dilution refrigerators use a pre-cooled mixture of two Helium isotopes, ^{3}He and ^{4}He, to achieve temperatures down to 2 mK. When cooled below a temperature of 870 mK, the two isotopes form a concentrated phase (practically 100 % ^{3}He) and a diluted phase (93.4 % ^{4}He, 6.6 % ^{3}He) through spontaneous phase separation [35].

Once in the mixing chamber, the coldest part of the cryostat, the two phases are in equilibrium, separated by a phase boundary. As the concentrated phase passes through the phase boundary into the diluted phase and

is diluted, heat is absorbed through endothermic dilution [35].

This type of cooling system is not designed for temperature control above 1 K. Thus, to measure in temperatures above 1 K, improvisation was needed. The refrigerator's cooling process is divided into several different stages. Stabilizing the temperature after each stage was tested and achieved. Thus, measurement temperatures in this system were 3.7 K, 1.0 K, 500 mK, 200 mK and 14 mK.

3.4.2 Helium pulse tube cryocooler

The second stage of measurements were those in temperatures above those available in the cryogen-free dilution refrigerator. Here, the cooling system was a Helium pulse tube cryocooler (PTC). The main components of PTCs are a cooling gas (here He), a piston that increases and decreases the pressure of the gas, and heat exchangers that allow heat to flow out and cooling power to flow in [35].

Figure 10 shows the cooled down, geometrically top-most part of the system, where the cold finger, hot stage and sample holder is located. When the system is in use, the cold finger is at a constant temperature. The hot stage heats up the system according to the temperature settings.

When the system first was tested for this experiment, the lowest temperature achieved was 43 K. This was higher than expected, as the cold finger should reach temperatures as low as 6 K. Since the highest temperature achieved in the cryogen-free dilution refrigerator is 4 K, reaching a minimum temperature closer to 4 K would be important to measure the whole temperature range.

In order to achieve this, the hot stage was removed and the copper cylinder connecting the hot stage to the sample holder was changed to a thinner cylinder. The aim of these changes was to reduce thermal loss. In addition, the Indium plate above the hot stage, and the Silver plate above the cold stage were replaced to new ones (plates not shown in Fig. 10). Here,

improved thermal conductivity was the aim.

After these changes, the system was tested again. The thermocouple in contact with the cold finger showed a temperature of 40 K, while the one at the sample holder showed 30 K. The reason to this inconsistency is most likely due to an error in either one or both of the thermocouples. Still, it can be concluded that the changes made to the system did result in a lower minimum temperature. However, it was hoped the changes would have closed the gap between measurement temperatures even more.

One measurement was made at this minimum temperature. In order to measure at higher temperatures, the hot stage was reinstalled. Measurements were then carried out at intervals of 10 K up to 100 K, and then with 50 K intervals up to 300 K. Temperature intervals were based on that Germanium is well-studied at temperatures above 100 K, and less so below.

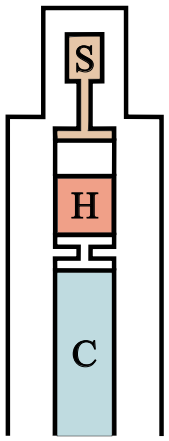

Figure 10: *Diagram of the part of the* >4 K *setup where the sample is placed. 'C' is the cold finger, 'H' is the hot stage, and 'S' is the sample and sample holder. The hot stage was removed for measurements at* 30 K.

3.5 Data analysis Methods

3.5.1 PALS

A lifetime spectrum is shown in Fig. 11. Before analysing the lifetime components, the background had to be subtracted and lifetime contributions from non-sample annihilations had to be determined and subtracted. The analysis methodology presented here is for a defect-free sample, as that is what was measured.

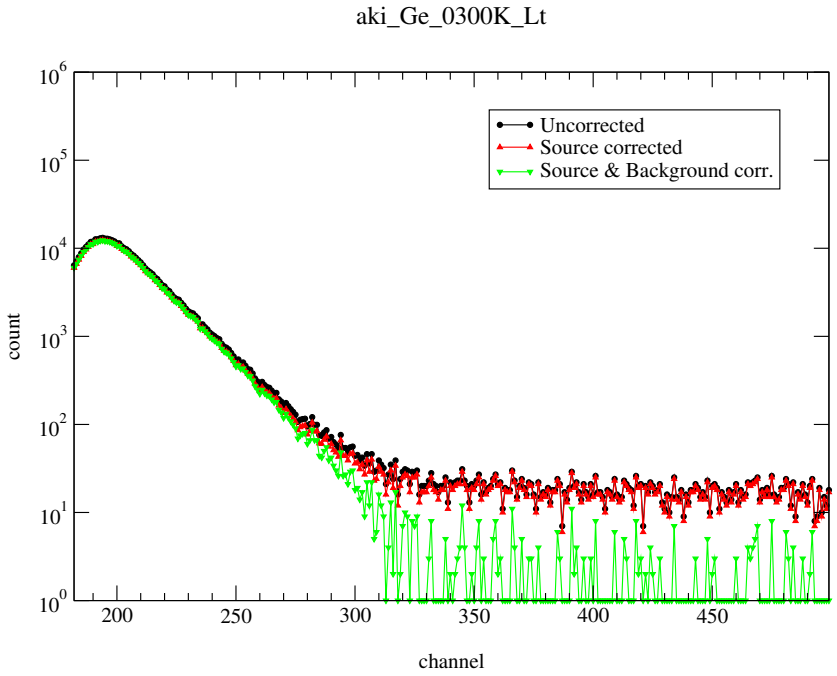

Figure 11: *Uncorrected, source corrected, and source and background corrected lifetime spectrum of Ge at* 300 K.

The lifetime analysis began by the calculation and subtraction of any lifetime components originating from annihilations outside the sample. There are three main unwanted lifetimes found in a lifetime spectrum that should be considered; annihilation events in the Al-foil, source annihilation events, and positronium annihilation events.

The Al foil lifetime is known to be 210 ps. The lifetime contribution was calculated using the Bertolini-Zappa formula:

$$k = 3.24 \times 10^{-3} \times Z^{0.93} \times s^{3.45/Z^{0.41}}, \tag{18}$$

where k is the fraction of positrons annihilation in the foil, Z is the atomic mass number of the measured sample and s is the foil thickness in mg/cm^2 [36]. The dependence of foil contribution on the atomic mass number originates from the positron backscattering coefficient η_+ previously discussed in the theory section of this thesis.

If the sample is a compound material, the weighted average of the atomic numbers should be used. Also, if the source is assembled in such a way that one or both sides are covered with more than one layer of foil, one should enter the thickness as the sum of the foil layers on that side. Then, the average of the foil contributions for both sides is calculated.

The source and positronium contributions to the mean positron lifetime are not calculated using a formula, as their intensities can vary, for example depending on the sample and on the activity of the source. Lifetime values for both components are known, so their intensity can be found through analysis. In analysis, the positron lifetime in the salt is assumed to be 400 ps and in positronium 1500 ps.

The positronium component should determined before the salt component. This begins by calculating an average background from the right-hand side of the spectrum. Next, the background is fitted by increasing the positronium intensity until the background matches the calculated average. Now, the positronium component of the lifetime has been found.

The final background-reducing step is to find the salt component. When running the analysis, two lifetime component intensities will be presented. One of them is the positron lifetime in the sample, while the other originates from the salt. Thus, the salt intensity component in the background reduction has to be increased until only one lifetime component is left in the

lifetime analysis.

In the case where the sample may contain defects, and thus other lifetime components, the process is similar. It starts with determining the Al-foil and salt components in a defect-free reference sample using the steps described above, and then using those correction values for the sample of interest. This way, more lifetime components can be fitted.

Since the obtained lifetime values are dependent on a few assumptions, estimations and calculations, there may be variations in obtained lifetime of approximately ± 2 ps. Nonetheless, through lifetime component fitting it is possible to find defects types present in the sample and their concentration. Often, the topic of interest is the change in lifetime as a function of e.g. temperature.

Normally, the the salt correction is determined only once and then used for all remaining measurements, as the salt correction is independent of temperature or other changes in the sample. However, the source that was used for the measurements at 14 mK-3.7 K was damaged, necessitating a change of source. Thus, the salt correction was determined twice; during analysis of the 14 mK measurement, and also for the 30 K measurement.

After all corrections have been performed, the remaining spectrum can be fitted. The average lifetime is found by calculating

$$\frac{1}{\lambda_{avg}} = \tau_{avg} \tag{19}$$

where λ_{avg} is the average annihilation rate. The average lifetime τ_{avg} also corresponds to the center of mass of the spectrum.

Since the sample measured in this thesis is defect-free, no additional lifetime components are expected. This is seen in Fig. 11; the lifetime curve after the peak is a straight line all the way down, instead of having different linear gradients along the curve. Note that the y-axis is logarithmic, and the gradients are in reality not linear, rather exponential.

3.5.2 Doppler Broadening

Data analysis in DBS is quite straightforward. First, the background has to be reduced from the raw spectrum. The background was calculated in Matlab. The background is not an even line across the spectrum, but higher on the left side than the right. Thus, the background was then calculated accordingly:

$$B_i = R_{avg} + (L_{avg} - R_{avg})\frac{N_{tot} - \sum_1^i (N_i)}{N_{tot}}, \tag{20}$$

where B_i is the calculated background at channel i, R_{avg} and L_{avg} are the average number of counts per channel on the right side and left side respectively of the peak (areas chosen by user), N_{tot} is the total amount of counts in the spectrum, and N_i is the number of counts in channel i. The background functional form is due to incomplete charge collection in the HPGe-detector.

After the background has been calculated it can be subtracted from the raw spectrum, as seen in Fig. 12. The background-reduced spectrum can then be analysed using previously discussed methods to obtain the S- and W-parameter.

As previously discussed, there is no set rule for defining the S- and W-parameter integration windows. However, to achieve a good statistical accuracy for the S-parameter, the window is typically chosen such that the area contains approximately 50 % of total counts.

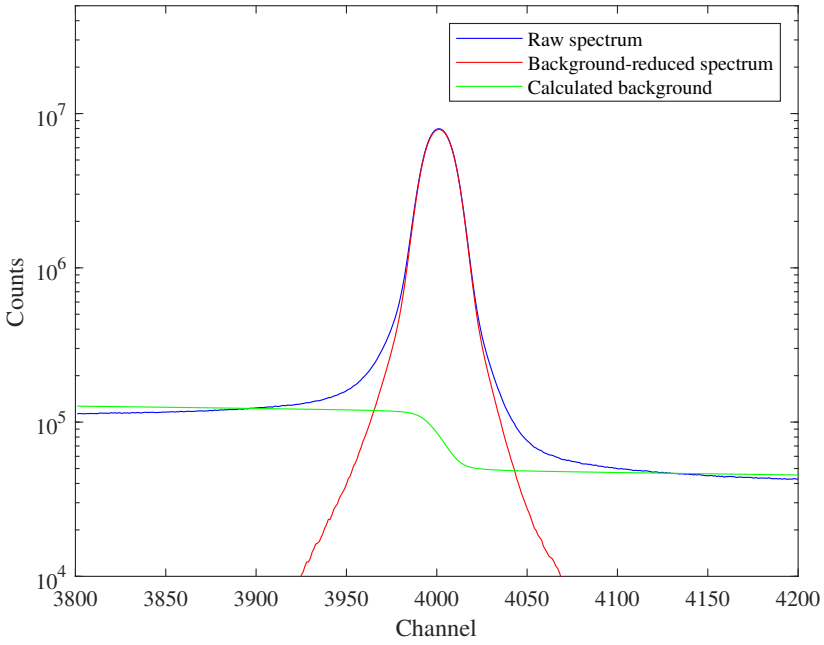

Figure 12: *Raw spectrum, calculated background, and background-reduced Doppler broadening spectrum of one of the Ge measurements.*

4 Results and Discussion

Since the Germanium sample only has a low amount of doping, there are also few defects present in the lattice. Thus, any observed changes in lifetime and Doppler Broadening with temperature are not attributed to defect mobility or recombination. Furthermore, these effects are expected to decrease in significance at low and, especially, at ultralow temperatures where mobility of atoms and defects significantly decreases.

As seen in Fig. 13 and Fig. 14, the S-parameter decreases with decreasing temperature, while the W-parameter increases with decreasing temperature, with the rate of change being greatest at the ultralow temperatures. This opposite behaviour between the S- and W-parameters is natural, since a wider annihilation line results in less counts in the center of the peak, and more in the wings. The data points at $T = 30\,\mathrm{K}$ and $T = 150\,\mathrm{K}$ clearly do not fit the trend of the rest of the data points. Thus, they have been treated as measurement errors and were ignored in this analysis.

In Fig. 15, the S- and W-parameters are shown in the interval of $14\,\mathrm{mK}$ to $50\,\mathrm{K}$. The temperature axis has been made logarithmic for easier trend visualisation. As seen in the graphs, the change in S- and W-parameter at ultralow temperatures is undoubtedly evidence of a real temperature-dependent process.

Since the S-parameter is a measure of annihilation events resulting in low-momentum photons, they are usually deduced to originate from positrons annihilating with valence electrons. Similarly, core electrons are the main contributor to the W-parameter. However, these deductions are made based on the assumption that the positrons have completed thermalization at the time of annihilation.

The drop in S-parameter with decreasing temperature seen in Fig. 13 and Fig. 15(a) can be explained by an increasing fraction of incomplete positron thermalization, and thus a greater total positron-electron momentum at the time of the annihilation event. A higher positron momentum also increases

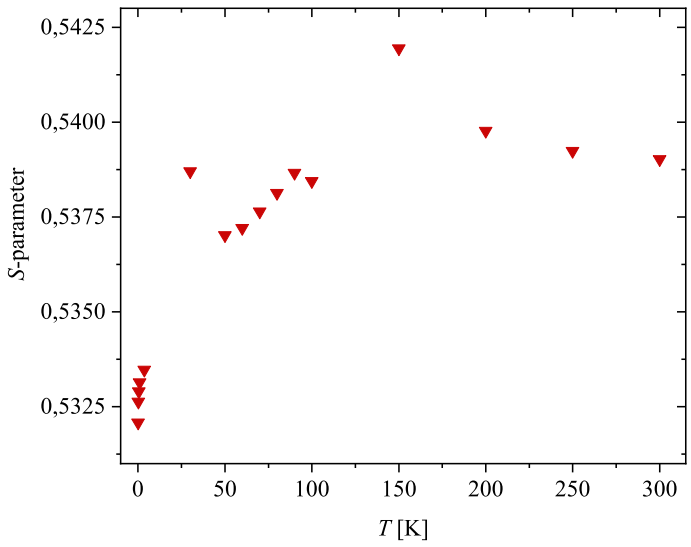

Figure 13: *S-parameter over the whole temperature range. The mean statistical error is* 7.94×10^{-5}*, and could thus not be displayed in the graph.*

the probability that the positron will annihilate with a core electron instead of a valence electron, further increasing the change in S-parameter. This is since a higher momentum allows the positron to get closer to the nucleus before the repulsive Coulomb force pushes it away.

Thermalization through electron-hole excitation with an energy less than the energy of the bandgap of the material is not possible. The bandgap of pure Ge increases from 0.66 eV at 300 K to 0.74 eV at 0 K. Thus, the energy loss mechanism of the positron converts to positron-phonon scattering earlier in the thermalization process, increasing thermalization time.

Figure 15 shows the average positron life as a function of temperature. As seen in the figure, not much can be deduced from the results; the lifetime seems to jump randomly from point to point, especially at the ultralow-temperature region. Here, data-acquisition time for one temperature was roughly four days due to the low count rate, much longer than an usual

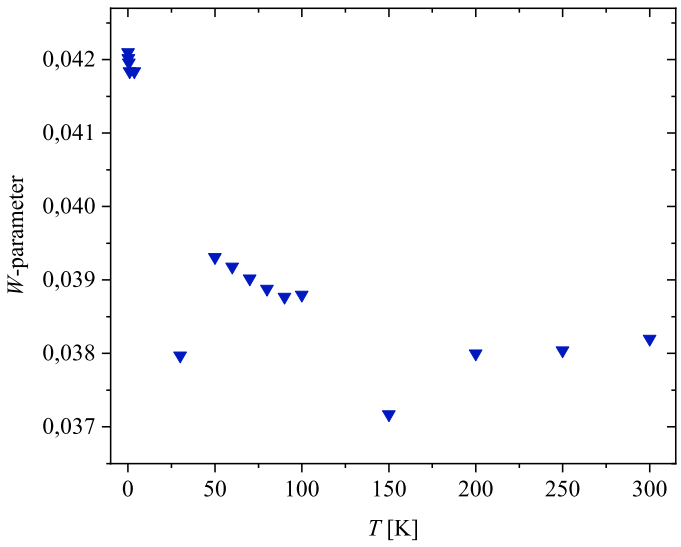

Figure 14: *W-Parameter over the whole temperature range. The mean statistical error is* 3.09×10^{-5}*, and could thus not be displayed in the graph.*

lifetime measurement. This can lead to statistical errors, e.g. by $t0$ drift. Also in the second stage of the measurements at high temperatures, data-aquisition time for one temperature was more than a day, which is longer than normal. In this region, even though there is no definite trend, the results seem to suggest no significant change in lifetime. This is in agreement with previous research.

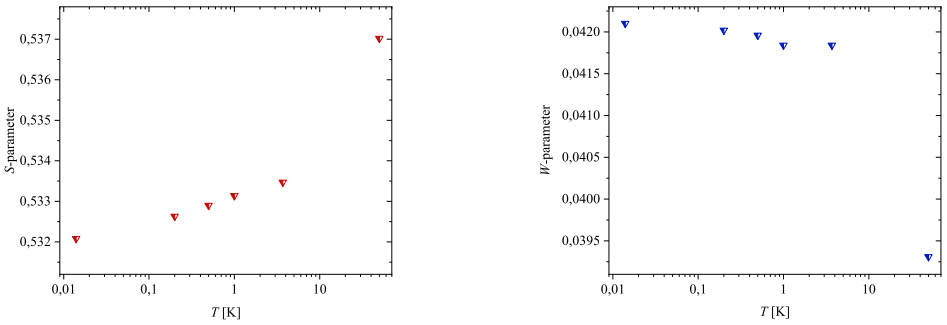

(a) S-parameter (b) W-parameter

Figure 15: *S-parameter and W-parameter plotted vs. logarithmic temperature in the temperature interval* 14 mK-50 K. *The* 30 K *data point has been left out due to aforementioned reasons.*

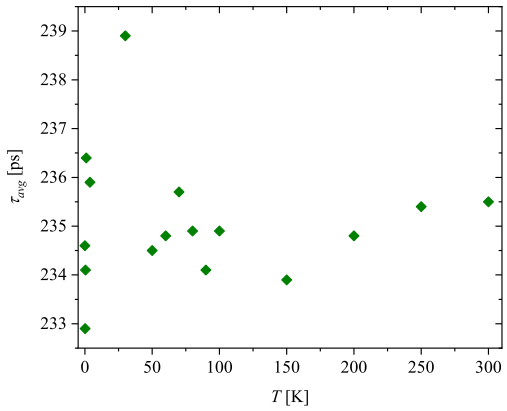

Figure 16: *Positron Lifetime*

5 Conclusion

The Doppler Broadening results presented in this thesis show some very interesting and novel phenomena occuring in the sample. Thermalization is most often assumed to be completed before annihilation. However, results presented in this thesis suggest this may not be the case at ultralow temperatures. The next step will be to determine why the probability of incomplete thermalization increases with decreasing temperature, and why this was observed here in a semiconductor but not in a metal in previous papers. Examples of possible areas of research are the effect of bandstructure, bandgap and phonon contribution on thermalization at ultralow temperatures.

This is also useful knowledge for future scientist wishing to examine semiconductors at these temperatures, even though such research is not common. Without this knowledge, changes in S- and W-parameter at ultralow temperatures might be attributed to defect behaviour instead of positron-sample processes. Naturally, this does not exclude any such processes, but merely encourages carefulness in analysis. For instance, results could be compared with defect-free samples if possible to examine the relative change.

Difficulties with the PALS setup and signal processing unfortunately prevented deeper analysis using this method. Previous research showed no change in positron lifetime over the whole temperature interval, and the same conclusion could possibly be made here. Considering incomplete thermalization and thus the positron diffusing through the lattice at a higher energy, this does not necessarily impact the positron lifetime. Still, to reduce the statistical limitations of future lifetime experiments, a new signal processing and analysis software is being developed to improve results obtained from the BaF_2 positron lifetime setup.

This thesis only investigates a small part of a large research field, and can thus be expanded. Results obtained in these experiments are not conclusive, and certainly are not guaranteed to apply to other materials or conditions. The author will continue the research by measuring Si, GaN, and Al. By

doing this, it will be possible to compare elemental semiconductors, compound semiconductors, and metals. In addition, an attempt will be made to obtain data points in the temperature range of 4K-30K, which currently was unachievable with the equipment used for these experiments.

Furthermore, it might be useful to repeat the Doppler Broadening measurements with a coincidence measurement setup. Coincidence setups consist of two collinear detectors, of which at least one is a HPGe-detector, and have significantly better peak-to-background ratio.

To summarise, in spite of many experimental challenges, this thesis work has produced definite experimental evidence of unexpected positron behaviour. Thus, even though positron annihilation spectroscopy techniques have been used for half a century, there may yet be undiscovered, fundamental processes of positrons at ultralow temperatures.

References

1. McCluskey, M. D. & Haller, E. E. *Dopants and Defects in Semiconductors, 1st Ed.* ISBN: 978-1439831526 (2012).
2. Dirac, P. A. M. The quantum theory of the electron. *Proc. Roy. Soc. Lond. A* **117,** 610–624 (1928).
3. Dirac, P. A. M. Quantised singularities in the electromagnetic field. *Proc. Roy. Soc. Lond. A* **133,** 60–72 (1931).
4. Anderson, C. D. The Apparent Existence of Easily Deflectable Positives. *Science* **76,** 238–239 (1932).
5. F. & Joliot-Curie, I. Un Nouveau Type de Radioactivité. *Comptes rendus des séances de l'Académie des Sciences* **198,** 254–256 (1934).
6. Beringer, R. & Montgomery, C. G. The Angular Distribution of Positron Annihilation Radiation. *Phys. Rev.* **61,** 222–224 (5-6 1942).
7. DeBenedetti, S., Cowan, C. E. & et al., W. R. K. On the Angular Distribution of Two-Photon Annihilation Radiation. *Phys. Rev.* **77,** 205–212 (2 1950).
8. Foster, P. J., Mascher, P. & et al., A. P. K. Implantation Profile of Na22 Continuous Energy Spectrum Positrons in Silicon. *Journal of Applied Physics* **101,** 043702 (2007).
9. Brandt, W. & Paulin, R. Positron Implantation-profile Effects in Solids. *Phys. Rev. B* **15,** 2511–2518 (5 1977).
10. Vries, J. D. *Positron Lifetime Technique with Applications in Materials Science* ISBN: 978-1439831526 (1987).
11. Krause-Rehberg, R. & Leipner, H. S. *Positron Annihilation in Semiconductors: Defect Studies* ISBN: 978-3-642-08403-4 (1999).
12. Perkins, A. & Carbotte, J. P. Effect of the Positron-Phonon Interaction on Positron Motion. *Phys. Rev. B* **1,** 101–107 (1 1970).

13. Jensen, K. O. & Walker, A. B. Positron thermalization and non-thermal trapping in metals. *Journal of Physics: Condensed Matter* **2,** 9757 (1990).

14. Jorch, H. H., Lynn, K. G. & McMullen, T. Positron Diffusion in Germanium. *Phys. Rev. B* **30,** 93–105 (1 1984).

15. Slotte, J., Makkonen, I. & Tuomisto, F. in *Characterisation and Control of Defects in Semiconductors* 263–288 (IET, 2019). ISBN: 978-1-78561-655-6.

16. Puska, M. J. & Nieminen, R. M. Theory of Positrons in Solids and on Solid Surfaces. *Rev. Mod. Phys.* **66,** 841–897 (1994).

17. Tuomisto, F. & Makkonen, I. Defect identification in semiconductors with positron annihilation: Experiment and theory. *Reviews of Modern Physics* **85,** 1583–1631 (2013).

18. Arifov, P. U., Grupper, A. R. & et al., H. A. *Coefficients of positron mass absorption and backscattering* in *Proc. 6th Int. Conf. Positron Annihilation* (1982), 699–701.

19. Czarnecki, A. & Karshenboim, S. G. *Decays of Positronium* in *14th International Workshop on High-Energy Physics and Quantum Field Theory* (1999), 538–544.

20. Kondev, F. G., Wang, M. & et al., W. J. H. The NUBASE2020 evaluation of nuclear physics properties. *Chinese Physics C* **45** (2021).

21. Hood, G. M. & Schultz, R. J. *Positron Annihilation in Aluminium at Low Temperatures* in *Proc. 5th Int. Conf. Positron Annihilation* (1979).

22. Schultz, P. J., Vehanen, A. & et al., W. T. Positron Annihilation in Al single crystals from 85 mK to 300 K. *Journal of Physics F: Metal Physics* **13,** L265 (1993).

23. Troev, T. & Pavlov, V. Positron Annihilation in aluminium at low and superlow temperatures. *Hyperfine Interaction* **80,** 999–1003 (1993).

24. Nissilä, J., Saarinen, K. & Hautojärvi, P. Positron thermalization in Si and GaAs. *Physical Review B* **63,** 165202 (2001).

25. Knoll, G. F. *Radiation Detection and Measurement, 4th Ed.* ISBN: 978-0-470-13148-0 (2010).

26. Scionix. *Physical properties of the most common scintillation materials* `https://scionix.nl/wp-content/uploads/2022/09/Physical-prop-scints.pdf`.

27. Saint-Gobain. *Barium Fluoride Scintillation Material* `https://www.crystals.saint-gobain.com/sites/hps-mac3-cma-crystals/files/2021-09/Barium-Fluoride-Data-Sheet.pdf`.

28. Lorenz, E., Mageras, G. & Vogel, H. Test of a Barium Fluoride Calorimeter with Photodiode Readout Between 2 and 40 GeV Incident Energy. *Nuclear Instruments and Methods in Physics Research Section A: Accelerators, Spectrometers, Detectors and Associated Equipment* **249,** 235–240 (1986).

29. National Institute of Standards and Technology. *Composition of Plastic Scintillator* `https://physics.nist.gov/cgi-bin/Star/compos.pl?refer=ap&matno=216`.

30. Rajainmäki, H. High-resolution Positron Lifetime Spectrometer with BaF2 Scintillators. *Appl. Phys. A* **42,** 205–208 (3 1987).

31. Sinha, B. & Bhattacharya, R. Reflectors for canning a BaF2 crystal. *Nuclear Instruments and Methods in Physics Research Section A: Accelerators, Spectrometers, Detectors and Associated Equipment* **276,** 237–241 (1989).

32. Klamra, W., Lindblad, T., Moszyński, M. & Norlin, L. Properties of optical greases for BaF2 scintillators. *Nuclear Instruments and Methods in Physics Research Section A: Accelerators, Spectrometers, Detectors and Associated Equipment* **254,** 85–87 (1987).

33. Hamamatsu. *Photomultiplier Tubes R2083, R3377* https://www.hamamatsu.com/content/dam/hamamatsu-photonics/sites/documents/99_SALES_LIBRARY/etd/R2083_R3377_TPMH1227E.pdf.

34. Hamamtsu R3378-51 product information sheet, delivered with the PMTs.

35. Waele, A. D. Basic Operation of Cryocoolers and Related Thermal Machines. *Journal of Low Temperature Physics* **164,** 179–236 (2011).

36. Bertolaccini, M. & Zappa, L. Source-Supporting Foil Effect on the Shape of Positron Time Annihilation Spectra. *Il Nuovo Cimento B* **52,** 487–494 (1967).